Modelling for understanding of COVID-19 spread and design of an isolation room in a hospital

Physics of Fluids

RESEARCH ARTICLE | FEBRUARY 07 2023

Modeling for understanding of coronavirus disease-2019 (COVID-19) spread and design of an isolation room in a hospital

Special Collection: Flow and the Virus

Xiaofei Wu (吴小飞) ; Hisham Abubakar-Waziri; Fangxin Fang ; Claire Dilliway ; Pin Wu (武频) ; Jinxi Li (李锦熙) ; Runming Yao (姚润明); Pankaj Bhavsar ; Prashant Kumar ; Christopher C. Pain ; Kian Fan Chung

Physics of Fluids 35, 025111 (2023)
https://doi.org/10.1063/5.0135247

AIP Publishing

Physics of Fluids ARTICLE scitation.org/journal/phf

Modeling for understanding of coronavirus disease-2019 (COVID-19) spread and design of an isolation room in a hospital

Cite as: Phys. Fluids **35**, 025111 (2023); doi: 10.1063/5.0135247
Submitted: 17 November 2022 · Accepted: 25 December 2022 ·
Published Online: 7 February 2023

Xiaofei Wu (吴小飞),[1,2] Hisham Abubakar-Waziri,[3] Fangxin Fang,[1,a)] Claire Dilliway,[1] Pin Wu (武频),[4] Jinxi Li (李锦熙),[5] Runming Yao (姚润明),[6] Pankaj Bhavsar,[3] Prashant Kumar,[7] Christopher C. Pain,[1] and Kian Fan Chung[3]

AFFILIATIONS

[1]Applied Modelling and Computation Group, Department of Earth Science and Engineering, Imperial College London, Prince Consort Road, London SW7 2AZ, United Kingdom
[2]Plateau Atmosphere and Environment Key Laboratory of Sichuan Province, School of Atmospheric Sciences, Chengdu University of Information Technology, Chengdu 610225, China
[3]National Heart and Lung Institute, Imperial College London, London SW3 6LY, United Kingdom
[4]School of Computer Engineering and Science, Shanghai University, Shanghai 200072, China
[5]Institute of Atmospheric Physics, Chinese Academy of Sciences, Beijing 100029, China
[6]Joint International Research Laboratory of Green Buildings and Building Environments (Ministry of Education), Chongqing University, Chongqing 400045, China
[7]Global Centre for Clean Air Research, Department of Civil and Environmental Engineering, Faculty of Engineering and Physical Sciences, University of Surrey, Guildford GU2 7XH, Surrey, United Kingdom

Note: This paper is part of the special topic, Flow and the Virus.
[a)]**Author to whom correspondence should be addressed:** f.fang@imperial.ac.uk

ABSTRACT

We have modeled the transmission of coronavirus 2019 in the isolation room of a patient suffering from severe acute respiratory syndrome coronavirus 2 (SARS-CoV-2) at the Royal Brompton Hospital in London. An adaptive mesh computational fluid dynamics model was used for simulation of three-dimensional spatial distribution of SARS-CoV-2 in the room. The modeling set-up is based on data collected in the room during the patient stay. Many numerical experiments have been carried out to provide an optimal design layout of the overall isolation room. Our focus has been on (1) the location of the air extractor and filtration rates, (2) the bed location of the patient, and (3) consideration of the health and safety of the staff working in the area.

I. INTRODUCTION

During the coronavirus disease 2019 (COVID-19) pandemic, a lot of attention has been given to the health risks and safety of indoor environments. Numerical models are a powerful tool for the estimation of the transmission risk of infectious diseases and of the role of ventilation needed to control transmission (Becker *et al.*, 2021; Foster and Kinzel, 2021; Mohamadi and Fazeli, 2022; and Zheng *et al.*, 2021). These models have the advantages of understanding virus and atmospheric processes, making predictions, uncertainty quantification, and optimal control/design. In numerical modeling, complex physical processes can be represented by partial differential equations. Mohamadi and Fazeli (2022) provide an overview of the applications of computational fluid dynamics (CFD) modeling for the COVID-19 pandemic. This includes the simulations of airborne virus dispersion by sneezing and coughing, the ventilation layouts, the effect of using or not using a face mask, virus inactivation by ultraviolet radiation, and the optimal location of virus sensors.

Hospital isolation rooms occupied by infectious patients represent a high airborne transmission risk environment for healthcare staff (Lindsey *et al.*, 2022). Hence, effective ventilation is key to providing a

safe environment for healthcare staff (Kumar *et al.*, 2022). The influence of ventilation on virus spread in isolation rooms has been widely studied with CFD simulations (Tsang *et al.*, 2023), including the position of the ventilation air inlet and outlet (Cheong and Phua, 2006; Ruiker *et al.*, 2021) and the air change rate (Wang *et al.*, 2021). A cough model was constructed to allow the numerical simulation of virus diffusion inside an isolation room for different ventilation system configurations. Shih *et al.* (2007) investigated the effects of a moving person and the opening and closing of a sliding door on room air distribution, including velocity, pressure, and contaminant fields with a dynamical mesh CFD, and suggested that the opening and closing of a sliding door has profound effects on internal pressure and velocity distributions. The position of the ventilation is crucial. Previous studies have shown that specific ventilation arrangements can minimize the impact of the virus transmission, such as in the study of airborne virus transmission in elevator cabins (Dbouk and Drikakis, 2021), restaurants (Li *et al.*, 2021), classrooms (Arjmandi *et al.*, 2022; Narayanan and Yang, 2021), hospital (Ruiker *et al.*, 2021), and underground stations (Kumar *et al.*, 2022).

This study focuses on modeling of virus transmission for a specified isolation room layout. Our objective is to provide guidance for isolation rooms containing patients being treated for COVID-19 pneumonia that will reduce the risk of virus infection, thus providing a safer and more comfortable work environment for healthcare staff. We have setup numerical simulations for different isolation room layouts and explored the situation with different locations of extractors and the rate of air exchanges in the room. An isolation room layout with the optimal reduction in the chance of being infected is shown.

II. AN ADAPTIVE MESH FINITE ELEMENT CFD MODEL FOR VIRUS TRANSPORT AND SPREADING

In this study, an adaptive mesh CFD model (named fluidity), developed at Imperial College London (http://fluidityproject.github.io/support.html), is used to simulate virus transport and spreading. Fluidity is a computational fluid dynamics code capable of numerically solving the following Navier–Stokes equation:

$$\frac{\partial \mathbf{u}}{\partial t} + \mathbf{u}\cdot\nabla\mathbf{u} = -\frac{1}{\rho}\nabla p + S_{\mathbf{u}} + \mu\nabla^2\mathbf{u}, \tag{1}$$

where $\mathbf{u} = (u, v, w)^T$ is the air flow velocity vector; t is the time; $\nabla = \frac{\partial}{\partial x}\mathbf{i} + \frac{\partial}{\partial y}\mathbf{j} + \frac{\partial}{\partial z}\mathbf{k}$; ρ is the (assumed uniform) density of the atmosphere; $S_{\mathbf{u}}$ represents the source, absorption, or the drag forcing term of velocity; and μ represents the dynamic viscosity. In this study, the room temperature is 20 °C, the air density $\rho = 1.23$ kg/m^3 and air dynamic viscosity $\mu = 1.825 \times 10^{-5}$ kg/ms. The mass conservation equation is given as

$$\frac{\partial \rho}{\partial t} = -\nabla\cdot(\rho\boldsymbol{u}). \tag{2}$$

The advection–diffusion field equation is used for modeling transport of temperature, humility, carbon dioxide (CO_2), and virus concentration

$$\frac{\partial C}{\partial t} + \nabla\cdot(\boldsymbol{u}C) - \nabla\cdot(\bar{\kappa}\nabla C) = S + D, \tag{3}$$

where C is the mass concentration of the virus, $\bar{\kappa}$ is the tensor of turbulent diffusivity, S represents the source term of virus, and D is the decay of virus; the decay term D can thus expressed as $D = -kC$. The virus exponential decay formulation (van Doremalen *et al.*, 2020) is given as follows:

$$C = C_0 \cdot e^{-kt}, \tag{4}$$

where C_0 is the initial virus concentration, and k denotes the decay rate. The decay of airborne viruses is sensitive to the meteorological conditions (Chan *et al.*, 2011; Dbouk and Drikakis, 2020; Schuit *et al.*, 2020; and Yang and Marr, 2012). The decay parameter for virus infectivity (min^{-1}) can be expressed as follows (Dabisch *et al.*, 2021):

$$k = 0.160\,30 + 0.040\,18\left(\frac{T-20.615}{10.585}\right) + 0.021\,76\left(\frac{RH-45.235}{28.665}\right) + 0.143\,69\left(\frac{S-0.95}{0.95}\right) + 0.026\,36\left(\frac{T-20.615}{10.585}\right)\left(\frac{S-0.95}{0.95}\right), \tag{5}$$

where T is the temperature (°C), RH is the relative humidity (%), and S is the integrated UVB irradiance (W/m^2). The effect of evaporation is not considered in this modeling (Ahmadzadeh *et al.*, 2021; Borro *et al.*, 2021; and Ren *et al.*, 2021). The initial background is taken from the measurement at the isolation room with no patient.

Fluidity employs the mixed continuous/discontinuous Galerkin finite element method for spatial discretization, and a time-stepping λ scheme is adopted for temporal discretization (here, the Crank–Nicolson scheme with $\lambda = 0.5$ is used). Here, we choose continuous Galerkin method for velocity and scaler variables while the control volume for pressure. For details of the characteristics and numerical schemes in fluidity, see Applied Modelling and Computation Group (2014). The Crank–Nicholson scheme is used here to ensure its robustness, unconditional stability, and second-order accuracy in time. The Navier–Stokes equation with the large eddy simulation (LES) and accompanying field equation is solved on arbitrary unstructured meshes. Anisotropic adaptive mesh techniques are employed in fluidity. The mesh is adapted to optimally resolve multi-scale flow dynamics in full three-dimension (3D) as the flow evolves in space and time. The air flow dynamic and virus transmission processes involve a wide range of spatial scales. An artificial dilution of viruses may lead to a shorter lifetime of the virus in existing fixed grid models if the resolution of grids is not high enough (Zheng *et al.*, 2015; 2020). The use of adaptive meshes can resolve multi-scale dynamic processes efficiently and effectively. The mesh is adapted with respect to the dynamic flow features and virus concentrations in time and space to provide maximum resolution in the most turbulent areas.

III. CASE STUDY: AN ISOLATION ROOM IN THE ROYAL BROMPTON HOSPITAL IN LONDON

A. Modeling setup

1. Study area

A typical isolation room 3401 in the Royal Brompton Hospital in London was studied, which is separated from the corridor by a lobby [see Fig. 1(a)]. The area of the room is 32.4 m^2. The room's thermometer reported 20 °C while the pressure stabilizer was operating which ensures that the pressure in the isolation room is lower by 10 Pa than that in the ventilated lobby. The air inlet is on the pressure stabilizer,

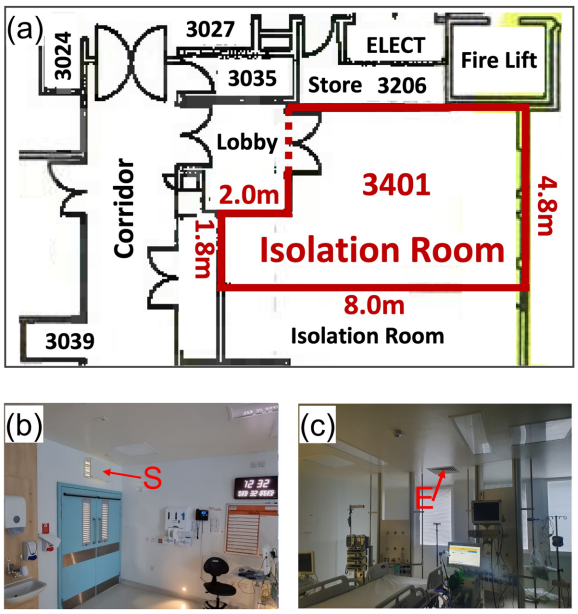

FIG. 1. The layout of Isolation Room 3401 at the Royal Brompton Hospital in London (provided by the Royal Brompton Hospital). S in (b) shows the location of the pressure stabilizer and buffer screen, and E in (c) indicates the location of the ceiling extractor.

but a baffle screen is mounted over the pressure stabilizer to prevent air jetting from the stabilizer [Fig. 1(b)]. In the simulation, the computational geometry of the room was generated using the Indoor Geometry Generator (IGG) tool developed by Mottet (2021) [shown in Fig. 2(a)]. A ceiling extractor [pink square, Fig. 2(b)] is installed as the air outlet, while the air inlet is on the pressure stabilizer [blue square, Fig. 2(a)].

2. Source locations and CO_2 concentrations

a. Assumptions

- The concentration of CO_2 is nearly uniform in the room when there are no patients.
- The concentration of CO_2 in the room is nearly equal to that in the corridor when there are no patients.
- The CO_2 emission rate from each patient is the same.
- The background of temperature and pressure is constant.
- The effect of droplet evaporation is not considered in our modeling study. Under normal circumstances, the cumulative amount of bio-aerosol produced by low frequency violent intermittent events of coughing and sneezing is much less than that of breathing and talking. Compared with a person intermittently coughing every minute, in the same period the simple act of breathing or talking produces ten times the amount of exhaled air (Gupta *et al.*, 2010). The behavior of particles resulting from these respiratory activities in the environment depends on their sizes, some of which are larger ($>5\,\mu$m) and are called droplets, and most of them are deposited by their gravity before they have a chance to evaporate. Some other smaller particles ($<5\,\mu$m), called aerosols, evaporate rapidly (Gralton *et al.*, 2011). Thus, the evaporation processes could be ignored when investigating the ventilation effects on virus transmission, for example, see the work of Ahmadzadeh *et al.* (2021), Borro *et al.* (2021), and Ren *et al.* (2021). Here, we do not consider the effect of the droplet evaporation but focusing on the effect of breathing alone. The droplet evaporation and particle matter processes will be included in our future work.

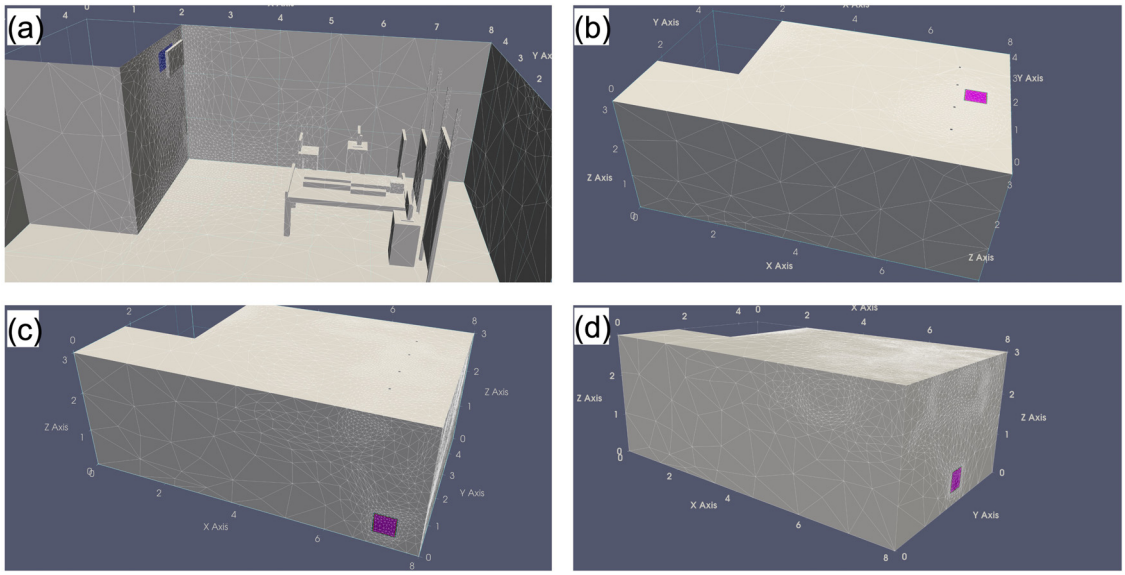

FIG. 2. The computational geometry and meshes of Isolation room 3401. The blue box in (a) indicates the inlet through which the air flow comes, and the pink boxes in (b), (c), and (d) indicate the location of the ceiling, south-wall, and east-wall extractor (outlet of the air flows), respectively.

TABLE I. Details of the experiments in this study.

Case ID	Case name	Air exchange (AC/h)	Extractor location	Number of mesh cells	Simulation time (h)
0	Exp_CTRL_10AC	10	Ceiling	199 309	53.9
1	Exp_CTRL_06AC	6	Ceiling	217 838	67.4
2	Exp_CTRL_14AC	14	Ceiling	305 301	79.7
3	Exp_South_10AC	10	South-wall	425 009	99.9
4	Exp_East_10AC	10	East-wall	417 710	97.9

b. Temperature. Initial and wall boundary condition: 20 °C, being referred to the temperature sensor in the isolation room; occupant head and breath temperature: 39 °C; body (covered with duvet): 23.5 °C (Bulińska and Buliński, 2015).

c. Relative humidity (RH). Initial condition and boundary condition at inlet: 45%, air exhaled by humans: 95%.

d. CO_2. Initial condition: 430 ppm (nearly observation in July 2021, without patient), boundary condition at inlet: 430 ppm, air exhaled by humans: 36 000 ppm.

3. Breath model

Bulińska and Buliński (2015) described the air flow rate at the mouth surface with sine function which is a good fit for the normal human breathing process,

$$\dot{Q}_b = a \sin(2\pi\omega t), \tag{6}$$

where ω is regular frequency, and $\omega = \frac{2\pi}{T}$, $\dot{Q}_b$ is the instantaneous volumetric flow rate exhaled by a human. Usually, a sedentary person or person performing light work exhales 6 l of air per minute with a frequency of ten breaths per minute (Hyldgaard, 1994). So that, T = 6 s,

$$\dot{Q}_b = 0.3141 \sin(1.047t). \tag{7}$$

We can, thus, obtain that the max velocity of the exhaled air flow is 2.66 m/s from a human mouth with an area of 1.18 cm^2.

a. CO_2 simulation without patients. Initial and inlet conditions: observed CO_2 concentration in an unoccupied isolation room.

b. CO_2 simulation with patients.

- Initial and inlet conditions: The same as CO_2 simulation without patients (based on the assumptions).
- Add CO_2 sources [Eq. (7)] at the patient's mouth.

c. Adaptive mesh resolutions. The use of dynamically adaptive meshes optimizes the computational effort to resolve the flow dynamic and virus transport processes over a wide range of spatial scales. In this study, the mesh is dynamically adapted with respect to both the wind velocity field and virus concentration. The *a priori* error measure for adapting the mesh is 0.3 m/s for velocity solutions and the relative error measure is 0.001 for the virus concentration. The minimum and maximum lengths of mesh are set to 0.02 and 1 m. The maximum number of cells is set at 600 000, which is large enough to ensure that the *a priori* error is achieved (see Table I). With the increasing number of cells used, the CPU time increases. For efficient simulations, the parametric non-intrusive reduced order model (P-NIROM) based on machine learning, proposed by Xiao *et al.* (2019) can be used in the future.

d. Simulation time. Calculations with sine wave model require a very small time step to fit the breathing cycle. The time step of all the simulations is set to 0.05 s so that one breath cycle could include 120 time steps. The whole simulation period is 15 min. The spin-up time is the first 10 min when the air flow and concentrations of CO_2 and virus come to a stable state. The time-averaged state over the last 5 min is analyzed in the following study.

e. Measurements. CO_2 monitoring was carried out continuously between 13 and 19 July 2020. The sensor was placed on the right side (from the patient's perspective) of the patient bed headboard at a height of 1.5 m. The measured CO_2 concentration is plotted in Fig. 3.

To validate the adaptive mesh virus model, we compare our numerical model results with the measurements with and without patients, shown in Fig. 4. Based on the record from the hospital, there is one patient in the room from 15:00 p.m. on 13 July to 17:00 p.m. on 15 July and from 2:00 a.m. to 8:00 a.m. on 18 July. The average CO_2 concentration is 461.6 ppm for the period with one patient and 421.7 ppm for the period without a patient.

It is seen that the CO_2 simulation results without patients are in a good agreement with the measurements while the modeling results slightly overestimate CO_2 with one patient in the room.

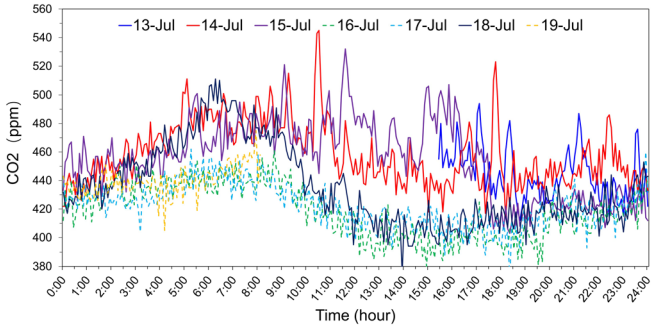

FIG. 3. Measurements of CO_2 during 13 – 19 July in 2020. There is one patient in the room from 15:00 p.m. on 13 July to 17:00 p.m. on 15 July (see the blue, red, and purple lines) and from 2:00 a.m. to 8:00 a.m. on 18 July (see the dark blue line).

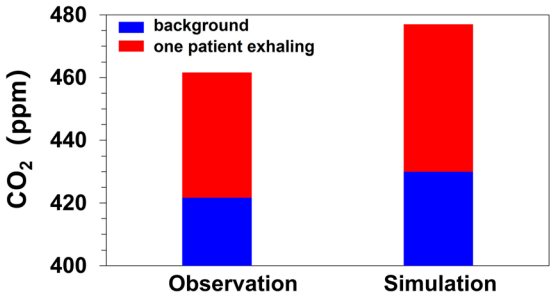

FIG. 4. Comparison of the average CO_2 concentration between measurements numerical results at the sensor location. The CO_2 concentration is averaged for the period with and without a patient.

B. Results and discussion

In this study, we aimed to provide the optimal layout for hospital isolation rooms. The study cases are depicted in Table I. The locations of the extractor are set on the ceiling, south-wall, and east wall (see Fig. 2) while the air exchange rates are 6, 10, and 14 air exchange per hour (AC/h) according to the standard of isolation rooms in the UK (Department of Health, 2007).

1. Spatial distribution of velocity field, temperature, and humidity

Virus lifetime is directly linked to the room environment, namely, the temperature and relative humidity. The decay rate can be calculated using Eqs. (4) and (5). The air velocity impacts how viruses are expelled from the patient's mouth and spread in the isolation room. To accurately model virus transmission in space and time, the mesh is adapted with respect to the solutions of variables (velocity and virus concentration), shown in Fig. 5(a). We can see that a high-resolution mesh is located at the air flow inlet and around the patient's head, as the velocity is very large at the inlet [Fig. 5(b)] and the virus concentration are high around the patient's head. Note that the meshes for the five experiments are adapted based on their own velocity and virus distribution, here just take Exp_CTRL_10AC as an example. The 3D distribution of the velocity vector is plotted in Fig. 5(b), and the air inlet and outlet are shown in Fig. 2. Figures 5(c) and 5(d) show the 2D spatial distributions of the temperature and RH of the cross section down the center of the patient's body. We can see an increased temperature around the patient's body while the highest RH (75%) is around the mouth, with a low RH value (40%) on the rest of the body. The 3D spatial distribution of virus concentrations is shown in Fig. 6. After the virus is emitted from the patient's mouth, it is driven largely in a vertical direction by buoyancy and wind forces. Relatively high concentrations (0.1–0.001) of viruses can be found within 1.4 m height above the bed [see Fig. 6(b)].

2. Effect of air exchange rates

To further investigate the impact of air exchange rates on virus transmission, three study cases have been setup with the air exchange rate of 6, 10, and 14 AC/h in the isolation room (see Table I). The 3D iso-surface of virus concentrations is plotted in Figs. 6(a)–6(c). The infectious area (the red representing the iso-surface of >0.1) of the virus emitted from the patient is largely concentrated at heights 0.7–2.1, 0.7–1.6, and 0.7–1.6 m for the air exchange rate of 6, 10, and 14 AC/h, respectively. The highest virus emission risk height is around 1.5 m. The horizontal contour map of the virus concentration at the height of 1.5 m is shown in Fig. 7. It is observed that the infectious area at 1.5 m high is the smallest in Case Exp_CTRL_AC10 with the air exchange rate of 10 AC/h. The effect of the ventilation rate can be seen from the 3D velocity distribution in the isolation room, shown in Fig. 8. With the increasing air exchange rate from 6 to 10 AC/h, the velocity speed increases along the virus transport path. The virus released from the patient is directly transported to the extractor. However, there is a recirculation flow near the extractor when the air

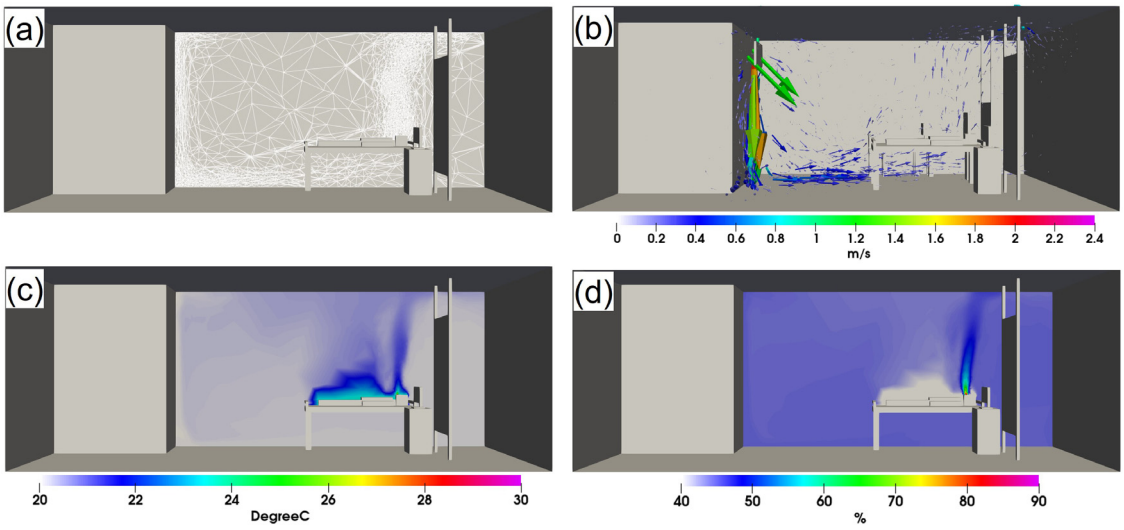

FIG. 5. The spatial distribution of (a) adaptive meshes, (b) velocity, (c) temperature, and (d) relative humidity.

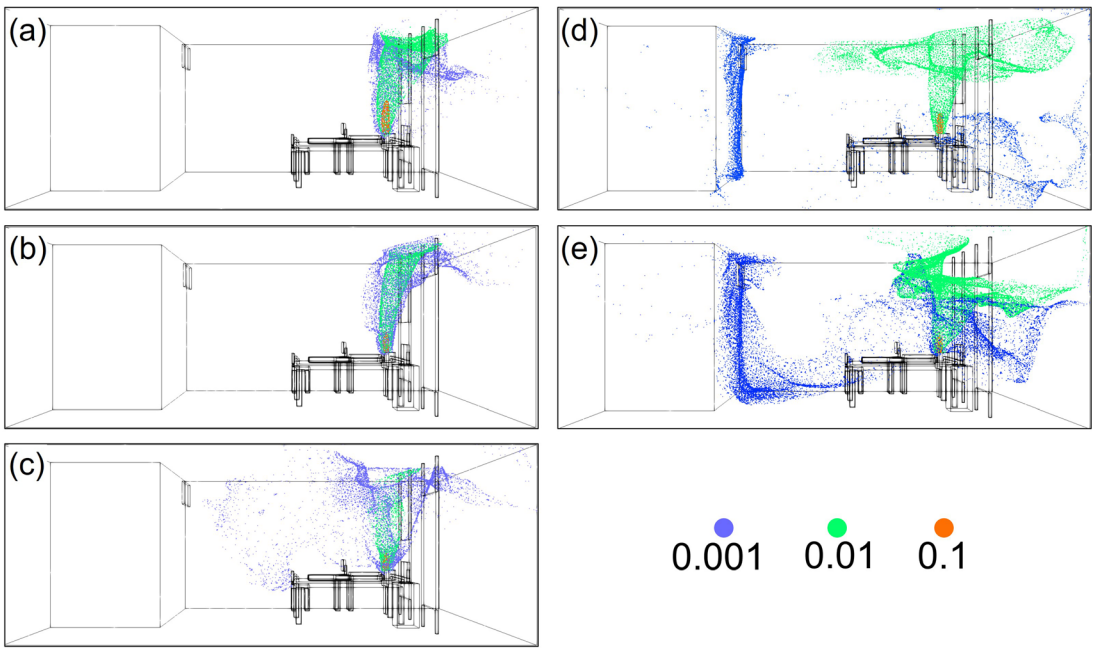

FIG. 6. 3D iso-surface of the virus concentration in the study cases: (a) Exp_CTRL_6AC, (b) Exp_CTRL_10AC, (c) Exp_CTRL_14AC, (d) Exp_South_10AC, and (e) Exp_East_10AC.

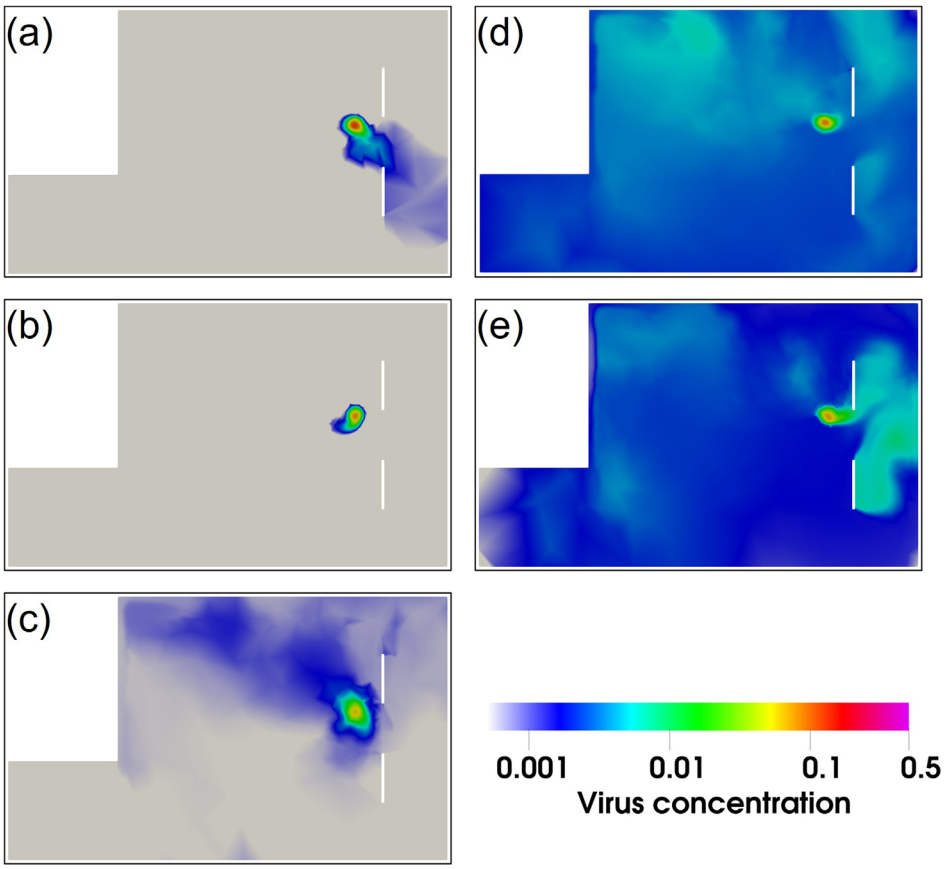

FIG. 7. The horizontal contour map of viruses at the height of 1.5 m in the studies cases: (a) Exp_CTRL_6AC, (b) Exp_CTRL_10AC with 10 AC/h, (c) Exp_CTRL_14AC, (d) Exp_South_10AC, and (e) Exp_East_10AC.

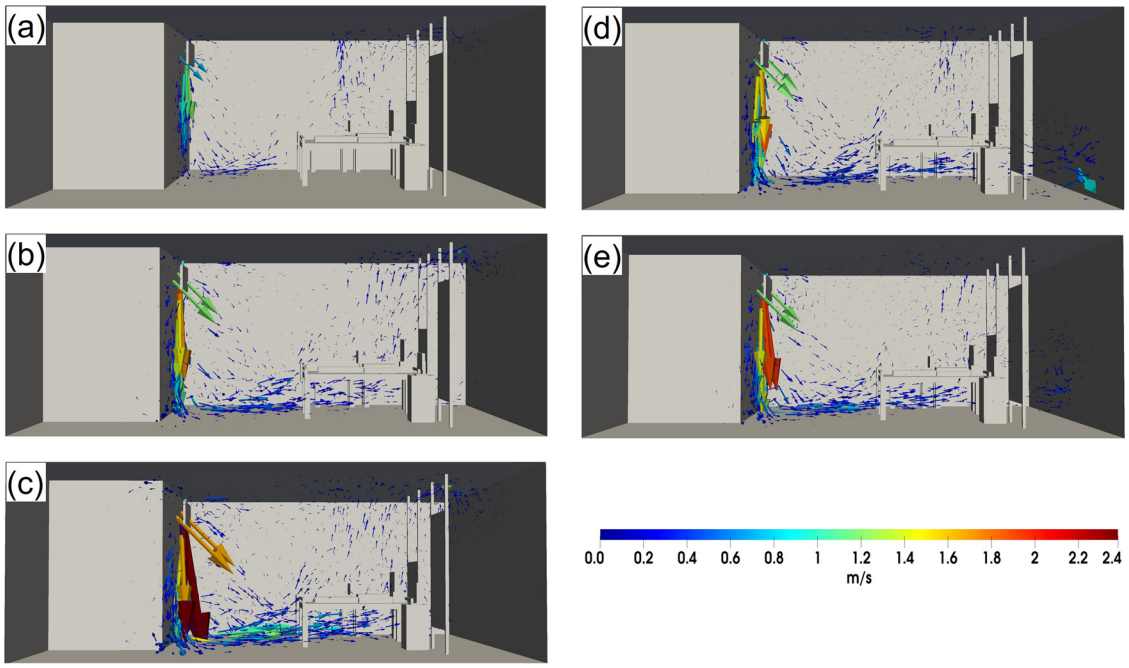

FIG. 8. 3D velocity vectors in the study cases: (a) Exp_ CTRL_6AC, (b) Exp_CTRL_10AC, (c) Exp_CTRL_14AC, (d) Exp_South_10AC, and (e) Exp_East_10AC.

exchange rate achieves 14 AC/h, which brings the virus back to the center of the room, thus leading to a larger infectious area than that with an exchange rate of 10 AC/h [see Figs. 7(b) and 7(c)]. It is, thus, argued that the optimal air exchange rate is 10 AC/h.

3. Optimal location of the extractor

The extraction location of the air outlet affects the transport path and infectious area of viruses. Three locations of the extractor were chosen: on the ceiling, south-wall, and east-wall at the height of 0.3 m (see Fig. 2). The 3D iso-surface of virus concentrations and horizontal contour map at 1.5 m high are shown in sub-figures (b), (d), and (e) of Figs. 6 and 7. It is clearly seen that the ceiling location of the extractor is the best for maximizing ventilation in the isolation room, where the infectious area is smallest compared to the other two locations. The virus emitted from the patient will immediately move upward due to the wind and buoyant forces. Obviously, the virus is directly blown out of the room if the extract is on the ceiling. Most of viruses remain within the room if the extractors are installed on the wall at a height of 0.3 m since there is a recirculation on the ceiling tracking the virus.

IV. CONCLUSIONS

In this study, we investigated the impact of the location of the extractor and air exchange rate on the risk transmission of the infectious virus, SARS-CoV2 in an isolation room in the Royal Brompton Hospital in London. For this study purpose, we have setup five cases with various air exchange rates and locations of the extractor. We found that the area with the highest risk of infection is on the top of the patient at a height of 0.7–2 m, where the highest concentration of the virus remains. For the study cases with a large air exchange (14 AC/h) and the extractor located on the east and south walls, there is a recirculation flow on the ceiling, thus leading to a larger infectious area. In summary, the optimal layout of the isolation room to minimize infection risk is to use the ceiling extractor and an air exchange rate of 10 AC/h. This study only focuses on an isolation room in a hospital. Note that the numerical results are limited due to the omission of droplet evaporation and particle matters. The evaporation and particle processes will be included our future model development. We will further investigate a standard patient room, intensive care unit, and waiting room in a hospital care setup in the future. Further work will also focus on AI-based surrogate modeling for rapid simulations, uncertainty analysis, and optimal control of ventilation systems as well as efficient energy use.

ACKNOWLEDGMENTS

This research was funded by the UK's Engineering and Physical Sciences Research Council funded projects: COVAIR (Grant No. EP/V052462/1), INHALE (Grant No. EP/T003189/1), Managing Air for Greener Inner Cities (MAGIC) (Grant No. EP/N010221/1), RELIANT (Risk EvaLuatIon, fAst iNtelligent Tool for COVID19, No. EP/V036777/1), MUFFINS (MUltiphase Flow-induced Fluid-flexible structure InteractioN in Subsea applications, No. EP/P033180/1), the PREMIERE programme grant (No. EP/T000414/1), and Rapid Assistance in Modelling the Pandemic (RAMP) project in the UK. We thank the support of staff at the Royal Brompton Hospital for measurements of Room 3401 and Laetitia Mottet for providing us the IGG tool to generate the

geometry. We would like to acknowledge the reviewers and Editor for their in-depth perspicacious comments that contributed to improving the presentation of this paper.

AUTHOR DECLARATIONS

Conflict of Interest

The authors have no conflicts to disclose.

Author Contributions

Xiaofei Wu: Conceptualization (lead); Formal analysis (lead); Investigation (lead); Methodology (lead); Software (lead); Validation (equal); Visualization (lead); Writing – original draft (equal); Writing – review & editing (lead). **Christopher Pain:** Funding acquisition (equal); Methodology (equal); Supervision (equal). **Fan K. Chung:** Data curation (equal); Formal analysis (equal); Funding acquisition (equal); Writing – original draft (equal); Writing – review & editing (equal). **Hisham Abubakar-Waziri:** Data curation (lead); Validation (supporting). **Fangxin Fang:** Conceptualization (equal); Funding acquisition (equal); Methodology (equal); Supervision (equal); Writing – original draft (equal); Writing – review & editing (equal). **Claire H. Dilliway:** Project administration (equal); Writing – review & editing (equal). **Pin Wu:** Conceptualization (equal); Methodology (equal). **Jinxi Li:** Conceptualization (equal); Methodology (equal); Writing – review & editing (equal). **Runming Yao:** Conceptualization (equal); Formal analysis (equal). **Pankaj Bhavsar:** Data curation (equal); Validation (supporting). **Prashant Kumar:** Conceptualization (equal); Investigation (equal); Writing – review & editing (equal).

DATA AVAILABILITY

The data that support the findings of this study are available within the article.

REFERENCES

Ahmadzadeh, M., Farokhi, E., and Shams, M., "Investigating the effect of air conditioning on the distribution and transmission of COVID-19 virus particles," J. Cleaner Prod. **316**, 128147 (2021).

Applied Modelling and Computation Group, Imperial College London, see http://fluidityproject.github.io/support.html for "Fluidity Manual." (2014).

Arjmandi, H., Amini, R., and Fallahpour, M., "Minimizing the respiratory pathogen transmission: Numerical study and multi-objective optimization of ventilation systems in a classroom," Therm. Sci. Eng. Prog. **28**, 101052 (2022).

Becker, A. D., Grantz, K. H., Hegde, S. T., Bérubé, S., Cummings, D. A., and Wesolowski, A., "Development and dissemination of infectious disease dynamic transmission models during the COVID-19 pandemic: What can we learn from other pathogens and how can we move forward?," Lancet Digital Health **3**(1), e41–e50 (2021).

Borro, L., Mazzei, L., Raponi, M., Piscitelli, P., Miani, A., and Secinaro, A., "The role of air conditioning in the diffusion of Sars-CoV-2 in indoor environments: A first computational fluid dynamic model, based on investigations performed at the Vatican State Children's hospital," Environ. Res. **193**, 110343 (2021).

Bulińska, A. and Buliński, Z., "A CFD analysis of different human breathing models and its influence on spatial distribution of indoor air parameters," Comput. Assisted Methods Eng. Sci. **22**(3), 213–227 (2015).

Chan, K.-H., Malik Peiris, J. S., Lam, S. Y., Poon, L. L. M., Yuen, K. Y., and Seto, W. H., "The effects of temperature and relative humidity on the viability of the SARS coronavirus," Adv. Virol. **2011**, 1.

Cheong, K. W. D. and Phua, S. Y., "Development of ventilation design strategy for effective removal of pollutant in the isolation room of a hospital," Build. Environ. **41**(9), 1161–1170 (2006).

Dabisch, P., Schuit, M., Herzog, A., Beck, K., Wood, S., Krause, M., Miller, D. *et al.*, "The influence of temperature, humidity, and simulated sunlight on the infectivity of SARS-CoV-2 in aerosols," Aerosol Sci. Technol. **55**(2), 142–153 (2021).

Dbouk, T. and Drikakis, D., "Weather impact on airborne coronavirus survival," Phys. Fluids **32**, 093312 (2020).

Dbouk, T. and Drikakis, D., "On airborne virus transmission in elevators and confined spaces," Phys. Fluids **33**, 011905 (2021).

Department of Health, *Health Technical Memorandum HTM 03-01: Specialized Ventilation for Healthcare Premises, Part A: Design and Validation* (Department of Health, Stationary Office London, 2007).

Foster, A. and Kinzel, M., "Estimating COVID-19 exposure in a classroom setting: A comparison between mathematical and numerical models," Phys. Fluids **33**(2), 021904 (2021).

Gralton, J., Tovey, E., McLaws, M.-L., and Rawlinson, W. D., "The role of particle size in aerosolised pathogen transmission: A review," J. Infection **62**(1), 1–13 (2011).

Gupta, R., Fletcher, D. F., and Haynes, B. S., "Taylor flow in microchannels: A review of experimental and computational work," J. Comput. Multiphase Flows **2**(1), 1–31 (2010).

Hyldgaard, C.-E., "Humans as a source of heat and air pollution," in *ROOMVENT '94, 4th International Conference on Air Distribution in Rooms*, edited by S. Mierzwinski (Silesian Technical University, Kraków, Poland, 1994), pp. 413–433.

Kumar, P. *et al.*, "Active air monitoring for understanding the ventilation and infection risks of SARS-CoV-2 transmission in public indoor spaces," Atmosphere **13**(12), 2067 (2022).

Li, Y., Qian, H., Hang, J., Chen, X., Cheng, P., Ling, H., Wang, S. *et al.*, "Probable airborne transmission of SARS-CoV-2 in a poorly ventilated restaurant," Build. Environ. **196**, 107788 (2021).

Lindsey, B. B. *et al.*, "Characterising within-hospital SARS-CoV-2 transmission events using epidemiological and viral genomic data across two pandemic waves," Nat. Commun. **13**, 671 (2022).

Mohamadi, F. and Fazeli, A., "A review on applications of CFD modeling in COVID-19 pandemic," Arch. Comput. Methods Eng. **29**, 3567–3520 (2022).

Mottet, L., see https://www.researchgate.net/profile/Laetitia-Mottet/publication/349350000_Indoor_Geometry_Generator_IGG_Manual/data/602c309f92851c4ed578ffa7/IGG-Manual.pdf. for "Indoor Geometry Generator (IGG) Manual" (2021).

Narayanan, S. R. and Yang, S., "Airborne transmission of virus-laden aerosols inside a music classroom: Effects of portable purifiers and aerosol injection rates," Phys. Fluids **33**(3), 033307 (2021).

Ren, J., Wang, Y., Liu, Q., and Liu, Y., "Numerical study of three ventilation strategies in a prefabricated COVID-19 inpatient ward," Build. Environ. **188**, 107467 (2021).

Ruiker, A., Mohammed, S., Chavan, R., Kumar, P., and Jadhav, S., "CFD modelling of contaminant control in designing ventilation system for an airborne infection isolation room (AIIR)," in *Proceedings of Building Simulation 2021: 17th Conference of IBPSA* (IBPSA, 2017).

Schuit, M. *et al.*, "Airborne SARS-CoV-2 is rapidly inactivated by simulated sunlight," J. Infect. Dis. **222**(4), 564–571 (2020).

Shih, Y.-C., Chiu, C.-C., and Wang, O., "Dynamic airflow simulation within an isolation room," Build. Environ. **42**(9), 3194–3209 (2007).

Tsang, T.-W., Mui, K.-W., and Wong, L.-T., "Computational fluid dynamics (CFD) studies on airborne transmission in hospitals: A review on the research approaches and the challenges," J. Build. Eng. **63**, 105533 (2023).

van Doremalen, N., Bushmaker, T., Morris, D. H., Holbrook, M. G., Gamble, A., Williamson, B. N., Tamin, A., Harcourt, J. L., Thornburg, N. J., Gerber, S. I., and Lloyd-Smith, J. O., "Aerosol and surface stability of SARS-CoV-2 as compared with SARS-CoV-1," N. Engl. J. Med. **382**, 1564–1567 (2020).

Wang, F., Chaerasari, C., Rakshit, D., and Permana, I., "Performance improvement of a negative-pressurized isolation room for infection control." Healthcare **9**(8), 1081 (2021).

Xiao, D. *et al.*, "Error estimation of the parametric non-intrusive reduced order model using machine learning," Comput. Methods Appl. Mech. Eng. **355**, 513–534 (2019).
Yang, W. and Marr, L. C., "Mechanisms by which ambient humidity may affect viruses in aerosols," Appl. Environ. Microbiol. **78**(19), 6781–6788 (2012).
Zheng, J., Zhu, J., Wang, Z., Fang, F., Pain, C. C., and Xiang, J., "Towards a new multiscale air quality transport model using the fully unstructured anisotropic adaptive mesh technology of fluidity," Geosci. Model Dev. **8**, 3421–3440 (2015).
Zheng, J., Fang, F., Wang, Z., Zhu, J., Li, J., Xiao, H., and Pain, C. C., "A new anisotropic adaptive mesh photochemical model for ozone formation in power plant plumes," Atmos. Environ. **229**, 117431 (2020).
Zheng, J. *et al.*, "Numerical study of COVID-19 spatial–temporal spreading in London," Phys. Fluids **33**(4), 046605 (2021).